Rigid boundary conditions for staggered-grid modelling

Zaiming Jiang (jianz@ucalgary.ca), John C. Bancroft, and Laurence R. Lines

ABSTRACT

Staggered-grid modelling methods have been shown previously to be more accurate than non-staggered grid schemes when liquids are involved inside the subsurface models. This report shows that the staggered-grid modelling can also accurately simulate seismic activities when rigid boundaries are involved:: the numerical modelling results accurately match the mathematical derivations and qualitative interpretations.

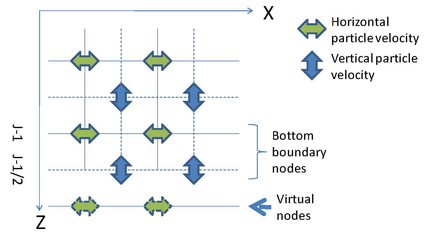

FIG. 2. For the bottom boundary a virtual line of nodes is put on the line *J*, outside of the subsurface model.

NUMERICAL MODELLING

Numerically, a rigid boundary for elastic modelling should be so designed that at the boundary the finite-difference estimates of both the horizontal and the vertical particle velocities (or displacements) are zero. Figure 2 shows a staggered-grid scheme with velocity / stress and time splitting but only particle velocity nodes are shown. taking the line *J-1/2* to be the rigid boundary, in addition to the values of vertical particle velocities on this line being set to zero, one should also assure that the horizontal particle velocities on this line to be equal to zero although there are no real numerical nodes on this line. If a virtual line of nodes is put on the line *J*, and the values on the virtual line are set anti-symmetric to those on the line *J-1, i.e.,*

$$U_J = -U_{J-1}. \qquad (3)$$

A 2D subsurface model is built to check the algorithm. The model is a homogeneous medium, with a rigid boundary at the bottom. The modelling results shown in Figure 3 accurately match the mathematical derivations and qualitative interpretations. The validity of the implementation method of the rigid boundary conditions within a staggered-grid modelling scheme is also proven.

MATHEMATICS

Mathematically, the reflections from a rigid boundary can be derived from rigid boundary conditions, which are the normal and tangential components of displacement must be zero. For the case of an incident P wave traveling inside a solid medium striking a rigid boundary, the amplitudes of reflected P- and SV-wave are

$$A_R = \frac{\cos(\theta+\phi)}{\cos(\theta-\phi)} A_I, B_R = -\frac{\sin(2\theta)}{\cos(\theta-\phi)} A_I. \qquad (1)$$

Where *A* and *B*, respectively, represent amplitudes of the P and SV waves; *I*, and *R*, the incident, and reflected waves; and θ and Φ, respectively, represent P and SV wave angles (Figure 1).

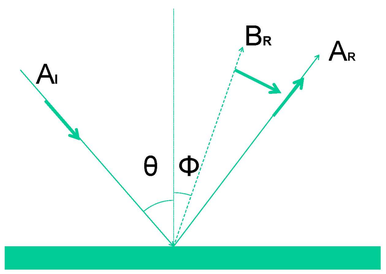

FIG. 1. An incident P wave traveling inside a solid medium striking a rigid boundary.

It can be predicted from equations (1) that

- There are both P and SV wave reflections when a P wave traveling in a solid medium strikes a rigid boundary at an incident angle other than zero;
- The amplitudes of P and SV wave reflections vary with the incident angle;
- The P wave reflection changes polarity at a certain wide incident angle shown in equations (2), which are derived by applying Snell's law.

$$\theta = \arctan\frac{V_p}{V_s}, \phi = \arctan\frac{V_s}{V_p}. \qquad (2)$$

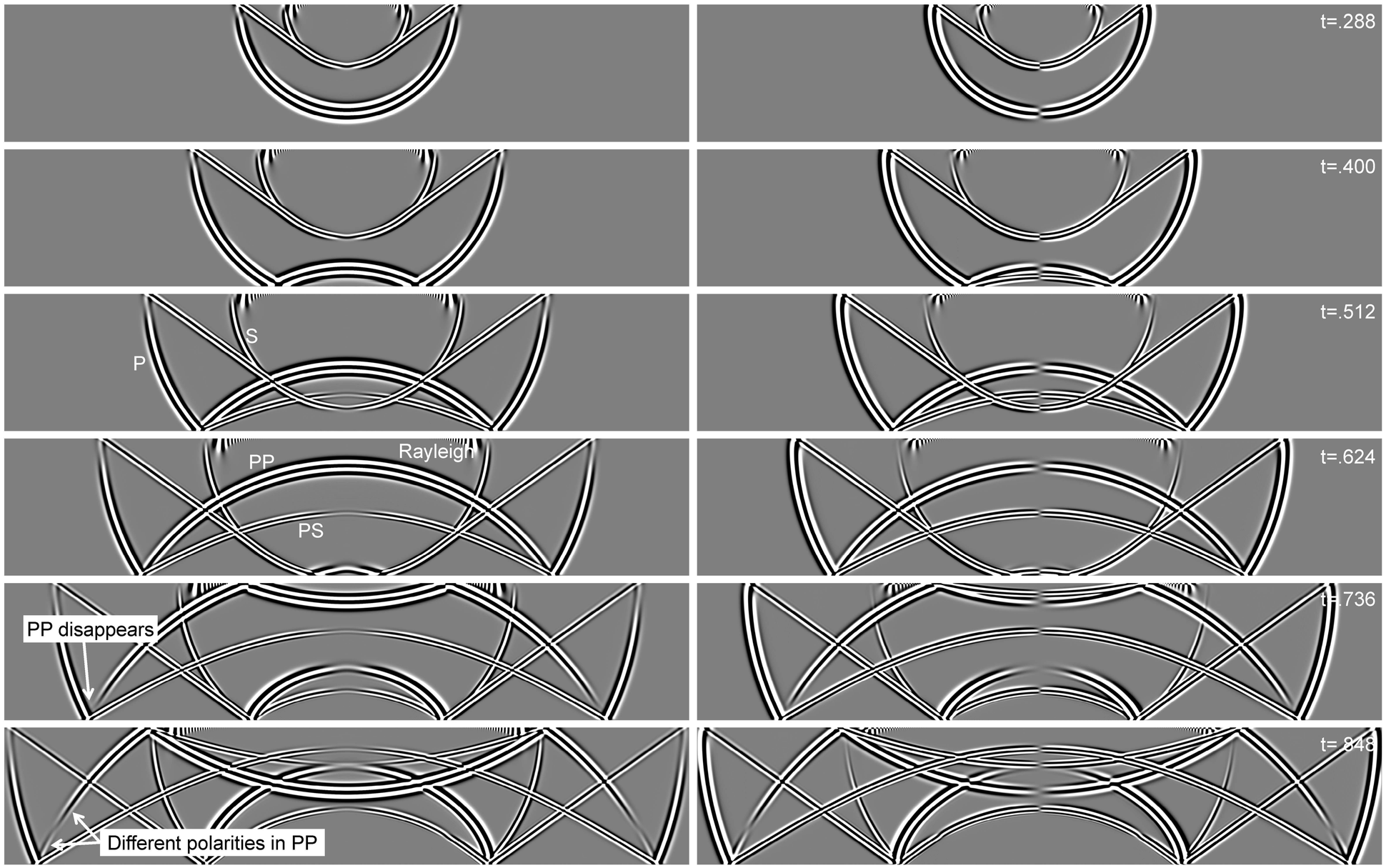

FIG. 3. Vertical (left column) and horizontal (right column) component snapshots of particle velocity data in time order. The source is at the centre of the surface, and the bottom is a rigid boundary. The unit for time is second. PP and PS, respectively, represents the P and SV wave reflections from an incident P wave. Since the P- and SV-wave velocities, respectively, 3,000 m/s and 1,732 m/s, according to equations (2), when P-wave incident angle is 60°, The PP reflection should disappear, which is confirmed in snapshots at t=.736s. At time 0.848s, with a greater P-wave incident angle, the PP reflection reappeares with a reversed polarity, which leads to two different polarities observable on the same wave front of the PP reflection, which was predicted mathematically.